Bulletin of the Seismological Society of America, Vol. 108, No. 2, pp. 801–814, April 2018, doi: 10.1785/0120170052

Spatiotemporal Variations of Ground Motion in Northern Chile before and after the 2014 M_w 8.1 Iquique Megathrust Event

by Jesús Piña-Valdés, Anne Socquet, Fabrice Cotton, and Sebastian Specht*

Abstract To evaluate the spatiotemporal variations of ground motions in northern Chile, we built a high-quality rock seismic acceleration database and an interface earthquakes catalog. Two ground-motion prediction equation (GMPE) models for subduction zones have been tested and validated for the area. They were then used as backbone models to describe the time–space variations of earthquake frequency content (Fourier and response spectra). Consistent with previous studies of large subduction earthquakes, moderate interface earthquakes in northern Chile show an increase of the high-frequency energy released with depth. A regional variability of earthquake frequency content is also observed, which may be related to a lateral segmentation of the mechanical properties of the subduction interface. Finally, interface earthquakes show a temporal evolution of their frequency content in the earthquake sequence associated with the 2014 Iquique M_w 8.1 megathrust earthquake. Surprisingly, the change does not occur with the mainshock but is associated with an 8 month slow slip preceding the megathrust.

Electronic Supplement: Strong-motion database.

Introduction

A key issue of seismic hazard assessment and engineering seismology is the capability to perform predictions of ground motions (e.g., peak ground acceleration [PGA] and response spectra) that can be generated by an earthquake at a specific site. With this aim, ground-motion prediction equations (GMPEs) have been developed to describe seismic response spectra of an earthquake. These models are generally parameterized for magnitude, fault type, distance (e.g., to the rupture plane), and site conditions (e.g., soil type). The models are presented in terms of a median and a standard deviation (e.g., Strasser *et al.*, 2009; Al Atik *et al.*, 2010; Haendel *et al.*, 2014). Several models have been derived for subduction zones (e.g., Youngs *et al.*, 1995, 1997; Zhao *et al.*, 2006; Abrahamson *et al.*, 2016). Because of the lack of data, most of these models have been developed using global databases that are mixing data from a couple of densely instrumented subduction zones (e.g., Japan, Alaska, Cascadia, Chile, and Mexico). The development of subduction ground-motion models then faces three main scientific challenges.

The first challenge is related to the regional variations of ground motions. Indeed, subduction zones are highly diverse in terms of mechanical behavior and geometry of the subduction interface (Kanamori, 1986; Astiz *et al.*, 1988; Tichelaar and Ruff, 1993; Heuret *et al.*, 2011). It is therefore necessary to evaluate regional variations of ground motions and test the robustness of global models for application to a given region.

The second challenge is related to the impact of interface earthquake depths on ground shaking. Recent observations of seismological data from megathrust earthquakes have shown that the slip properties and spectral content of waves generated by major subduction events are highly depth dependent (e.g., Lay *et al.*, 2012). These new observations challenge the ability of GMPEs to take into account the impact of depth on ground motions of interface earthquakes of moderate M_w, which are excluded from past subduction GMPE models. Such moderate earthquakes ($M_w < 5$) have a limited impact on seismic hazard assessment, which is mainly controlled by large earthquakes. They may however provide key information on the regional variations of the subduction interface properties and associated segmentation.

The third challenge relates to the impact of the processes at stake on the subduction interface during a seismic cycle on the generated ground motions. Recent major subduction earthquakes have also shown long (several years) preparation phases (Bouchon *et al.*, 2013; Schurr *et al.*, 2014) and post-seismic phases (Ozawa *et al.*, 2012; Mavrommatis *et al.*,

*Also at Section 2.6 Seismic Hazard and Stress Field, GFZ German Research Institute for Geosciences, Helmholtzstrasse 6, 14467 Potsdam, Germany.

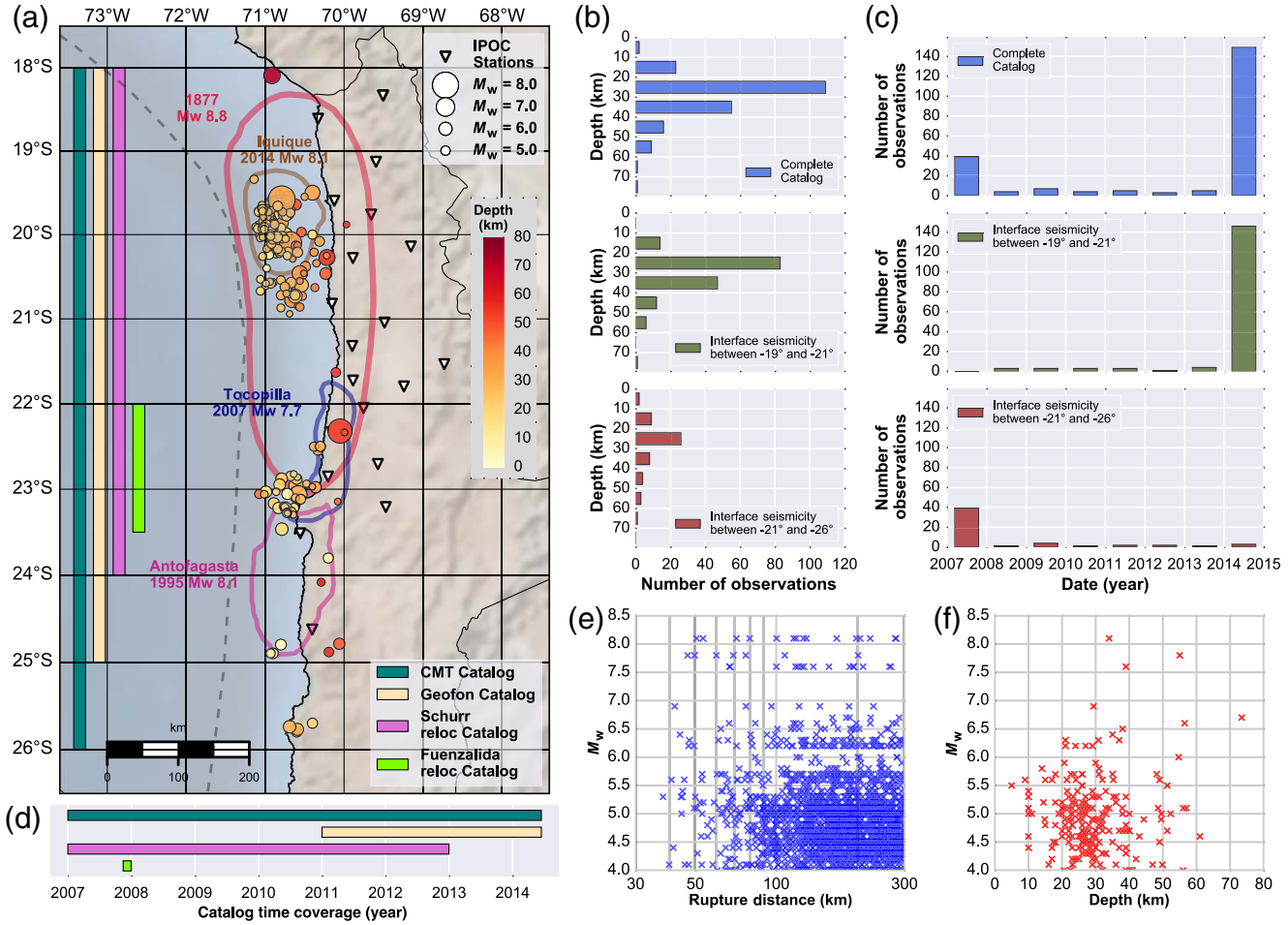

Figure 1. (a) Spatial distribution of the interface seismicity; the circles indicate the epicenter location, the fill indicates the depth, and the size indicates the magnitude. Contours of recent megathrust earthquakes ruptures are shown. Inverted triangles show the distribution of Integrated Plate boundary Observatory Chile (IPOC) multiparameter stations. Observed seismicity is concentrated in two clusters: the first one is centered at latitude −20° and the second one at −23°. The vertical bars on the left of the map indicate the latitudinal coverage of the catalogs included in the compilation used in this study. (b) Histograms of seismicity depth distribution and (c) histograms of seismicity temporal distribution, for whole catalog (upper), northern cluster (middle), and southern cluster (bottom). Most of the seismic activity occurs between 10 and 60 km depth. North cluster is mostly composed by the foreshock and aftershock sequences of the 2014 Iquique earthquake (M_w 8.1), and the southern cluster by the aftershock sequence of the 2007 Tocopilla earthquake (M_w 7.7). (d) Time coverage of the different catalogs. (e,f) Distribution of M_w as a function of rupture distance and depth, respectively. The color version of this figure is available only in the electronic edition.

2015; Yokota and Koketsu, 2015; Cesca *et al.*, 2016; Kato *et al.*, 2016). Variations of the frictional properties of the plate interface are likely associated with these preseismic and postseismic phases, and may cause ground-motion temporal variations. However, these ground-motion time dependencies have not yet been analyzed.

The northern Chile subduction (Fig. 1, left) provides a good case study to analyze regional, depth, and time dependencies of ground motions. The high convergence rate of 65–70 mm/yr between the Nazca and South American plates (Argus *et al.*, 2011) generates observed seismicity associated with the interface plate convergence. This zone can be seen as a mature seismic gap between −23° and −18°S of latitude, as it has experienced only partial ruptures since the 1877 M_w 8.8 megathrust earthquake (Lomnitz, 2004). In 2007, the M_w 7.7 Tocopilla earthquake broke the deeper portion of subduction interface at the southern part of the gap (Delouis *et al.*, 2009; Béjar-Pizarro *et al.*, 2010; Motagh *et al.*, 2010; Peyrat *et al.*, 2010). In 2014, the M_w 8.1 Iquique earthquake partially ruptured an ∼150-km-long portion of the subduction interface centered at 20° S of latitude (Ruiz *et al.*, 2014; Schurr *et al.*, 2014; Gusman *et al.*, 2015), with a coseismic moment release less than half of the moment deficit estimated in the area (Béjar-Pizarro *et al.*, 2013; Métois *et al.*, 2013, 2016; Hayes *et al.*, 2014).

Because this region is identified as a high seismic hazard region, an important effort of seismological and geodetic monitoring has been performed since 2006 by several international agencies. In particular, 21 permanent multiparameter stations (including broadband seismometer, acceler-

ometer, and Global Positioning System) have been installed in the frame of the Integrated Plate boundary Observatory Chile (IPOC) on relatively homogeneous rock geotechnical conditions. This network provided a substantial seismic catalog and associated high-quality rock-site conditions and strong-motion records, which are suitable to test GMPE models and also characterize the spatial and time variations of the earthquakes ground motion in this area. Thus, given this dataset, relevant GMPEs can be tested for their applicability to ground-motion estimates for the region.

Interface Earthquake Catalog

Having a reliable earthquake catalog is a critical point to analyze ground motions. Building a good catalog with a limited level of unknowns can potentially reduce the uncertainty of the ground motion predicted by the GMPEs. Indeed, earthquake catalogs provide most of the key parameters necessary to apply the GMPEs such as event location and magnitude. In addition, information about fault-plane orientation derived from earthquake focal mechanisms allow the style of faulting to be discriminated, key information to evaluate whether the event occurred on the subduction interface or within the subducted slab.

To compile a seismic catalog of interface seismicity appropriate for our purpose, we have searched events with $M_w \geq 4.0$ between January 2007 and June 2014, within the region between 18°–26° S and 69°–72° W of latitude–longitude range. We only considered events with a maximum depth of 90 km and with available focal mechanism solutions (FMS). Our catalog is a compilation of four different catalogs characterized by different accuracies and precisions of the hypocenter location, and different coverage in time and space (Fig. 1a,b). We selected data associated with each earthquake from the most accurate catalog. The four databases below are sorted from most to least accurate:

1. High-resolution relocated catalog of the 2007 Tocopilla seismic event (Fuenzalida *et al.*, 2013): magnitude, hypocentral location, and focal mechanism of 31 aftershocks, following the14 November 2007 M_w 7.7 Tocopilla earthquake. The catalog includes earthquakes located between 21° and 24° S, within 45 days after the mainshock.
2. Relocated catalog of north Chile (Schurr *et al.*, 2012): magnitude and hypocentral location of 106 earthquakes from January 2007 to December 2012, within 18°–25° S and 69°–72° W, estimated from records of IPOC permanent stations.
3. GEOFON data center (GFZ) catalog (automatic estimates): magnitude, hypocentral location, and focal mechanism of 245 earthquakes from January 2011 to June 2014 within 18°–25° S and 69°–72° W, estimated from records of IPOC permanent stations.
4. Global Centroid Moment Tensor: magnitude, hypocentral location, and focal mechanism of 89 earthquakes from January 2007 to June 2014, within 18°–26° S and 69°–72° W.

The seismicity in the obtained catalog has been classified as either interface or intraplate earthquakes based on FMSs, using the Angular Classification with Expectation–Maximization cluster analysis (Specht *et al.*, 2017), resulting in 216 identified interface earthquakes. We checked that this data-driven cluster analysis gave consistent classification results with the classical expert classification based on earthquake location and focal mechanisms used by Bastías and Montalva (2016). Additionally, 112 earthquakes that are not included in the catalog of Bastías and Montalva (2016) were identified, which correspond mainly to earthquakes of M_w between 4 and 5 that are not included in their work.

In the studied time period, the interface seismicity occurred in two main clusters (Fig. 1a). The cluster located south of the gap (~23°S of latitude) is related to the 2007 M_w 7.7 Tocopilla earthquake. The cluster located between 19° and 21° S of latitude is related to the seismic event of the 2014 M_w 8.1 Iquique earthquake, and contains most of the seismicity included in our catalog. Both of them show depths between 10 and 60 km (Fig. 1b), and are highly concentrated in the years 2007 and 2014, respectively (Fig. 1c).

Acceleration Database and Data Processing

Multiple strong-motion databases are available in Chile (e.g., Arango *et al.*, 2011; Bastías and Montalva, 2016). We have however chosen to use only the IPOC data to use homogeneous rock-site data to characterize the spatiotemporal variations of earthquakes frequency content, and also perform GMPE testing using an independent dataset.

Processing the acceleration dataset has been performed following the guidelines and recommendations of the COSMOS strong-motion record workshop (Boore and Bommer, 2005). We used horizontal acceleration records of interface events with a sampling frequency of 100 Hz. Records were cut 100 s before and 300 s after the reported event time. The raw data were deconvolved before applying a standard correction procedure. First, a baseline correction was performed by detrending and demeaning the acceleration time series to remove the instrument offset. Then, the records were manually picked to define the beginning and the end of the relevant seismic signal. Finally, the signal was tapered and zeros were padded at the beginning and the end of the waveform following Akkar *et al.* (2014).

The acceleration response spectra have been calculated over the north–south and east–west components, at 5% spectral damping ratio (Ⓔ Table S1, available in the electronic supplement to this article), using the method proposed by Nigam and Jennings (1969). The horizontal acceleration response spectrum was then obtained by calculating the geometric mean of the response spectra of both horizontal components for each oscillator of fundamental period T, as

$$SA_{hor}(T) = \sqrt{SA_{NS}(T) \times SA_{EW}(T)}, \qquad (1)$$

in which SA_{NS} and SA_{EW} correspond to the acceleration response spectra of the north–south and east–west acceleration

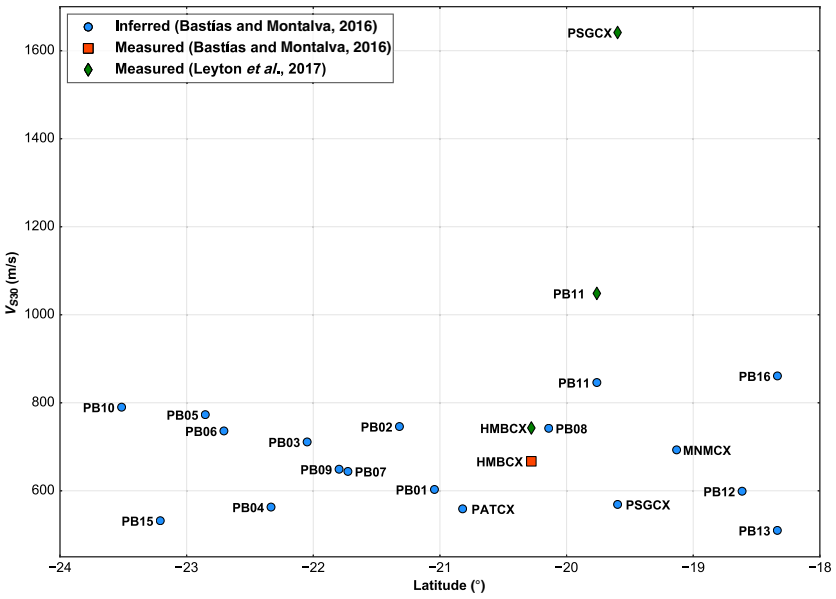

Figure 2. Average of the top 30 m shear-wave velocities (V_{S30}) of the CX-network stations with respect to the latitude. The square and circles indicate the measured and inferred V_{S30} values, respectively, taken from Bastías and Montalva (2016). Diamonds show the measured values taken from Leyton *et al.* (2017). Note that the station PB13 has been replaced by the station PB16 (located near to the original site). This new station shows an inferred V_{S30} 69% higher than the PB13 site. The color version of this figure is available only in the electronic edition.

components, and SA_{hor} corresponds to the horizontal response spectra.

Evaluation of Ground-Motion Prediction Equations

We tested two GMPEs for subduction environments: the Abrahamson *et al.* (2016) model, which is a current GMPE model that has been calibrated with a worldwide database, and the Montalva *et al.* (2017) model that has been calibrated with a local ground-motion database of earthquakes of M_w higher than 5, exclusively occurring on the Chilean subduction zone between −34° and −17° of latitude, including the records of the IPOC stations.

Because we have no rupture plane models for the events, we estimate the rupture plane distance (R_{rup}), which is defined as the minimum distance between the rupture plane and a given site, by estimating the position and orientation of a rupture plane from the hypocentral depths and the dip and strike given by the focal mechanisms. Because focal mechanisms have two nodal planes, we selected the nodal plane that is (near) parallel to the subduction interface as the rupture plane. As generally there is no information about the hypocenter position relative to the rupture plane, we assumed the hypocenters to be located at the center of the rupture planes and its geometry defined by the scaling relations of rupture source proposed by Strasser *et al.* (2010). Finally, a grid was defined on each rupture plane, to search the minimum distance between the nodes of the grid and the station site. When the minimum is localized, a refined grid is defined around the location of the minimum and the process is repeated again until no significant variations are observed (Haendel *et al.*, 2014; Bastías and Montalva, 2016). The result of this procedure is summarized in Figure 1e that shows the magnitude–rupture distance distribution from 40 to 300 km for the whole range of magnitudes of the catalog.

Both selected GMPE models require the V_{S30} value to estimate indirectly the site effects on ground motions. There is no specific geotechnical information for the whole IPOC Network. Such lack of information has been supplied in previous works using proxy-based estimation on the predominant frequencies and the topographical slope (e.g., Bastías and Montalva, 2016). These inferred values are however lower than measured V_{S30} values obtained recently at the stations HMBX, PSGX, and PB11 by Leyton *et al.* (2017) (Fig. 2). Additionally, stations PB16 and PB13 (separated by a distance no larger than 500 m) show significant differences of their inferred V_{S30} values. Such discrepancies between inferred and measured values confirm that a solid characterization of IPOC site conditions would lead to a significant improvement of the network.

Considering the discrepancy between inferred and measured values of V_{S30}, the homogeneity of geotechnical conditions of sites and the consistence between their geotechnical description and the measured values, a conservative value of V_{S30} of 850 m/s has been adopted for all stations of the network, similar to the value assumed by Haendel *et al.* (2014). This assumption will be tested later in the article by the computation of site-specific stations terms and their comparisons with inferred V_{S30}.

Using this information and the data of the earthquake catalog, we calculated the predicted acceleration response spectra for each station–earthquake pair, for PGA and three different oscillator periods (0.1, 0.8, and 1.33 s). The respective values of the GMPEs were then compared with the observed horizontal accelerations response spectra for the given oscillator periods to compute the total normalized residuals as

$$Z_T^{ij}(T) = \frac{\log[SA_{obs}^{ij}(T)] - \log[SA_{pred}^{ij}(T)]}{\sigma(T)}, \qquad (2)$$

in which $Z_T^{ij}(T)$ is the residual at site j for event i with oscillator period T, $SA_{obs}^{ij}(T)$ and $SA_{pred}^{ij}(T)$ correspond to the observed and predicted acceleration response spectra at site j for event i with oscillator period T, respectively, and $\sigma(T)$ is the total standard deviation of the model for oscillator period T. These residuals have been calculated only for the records

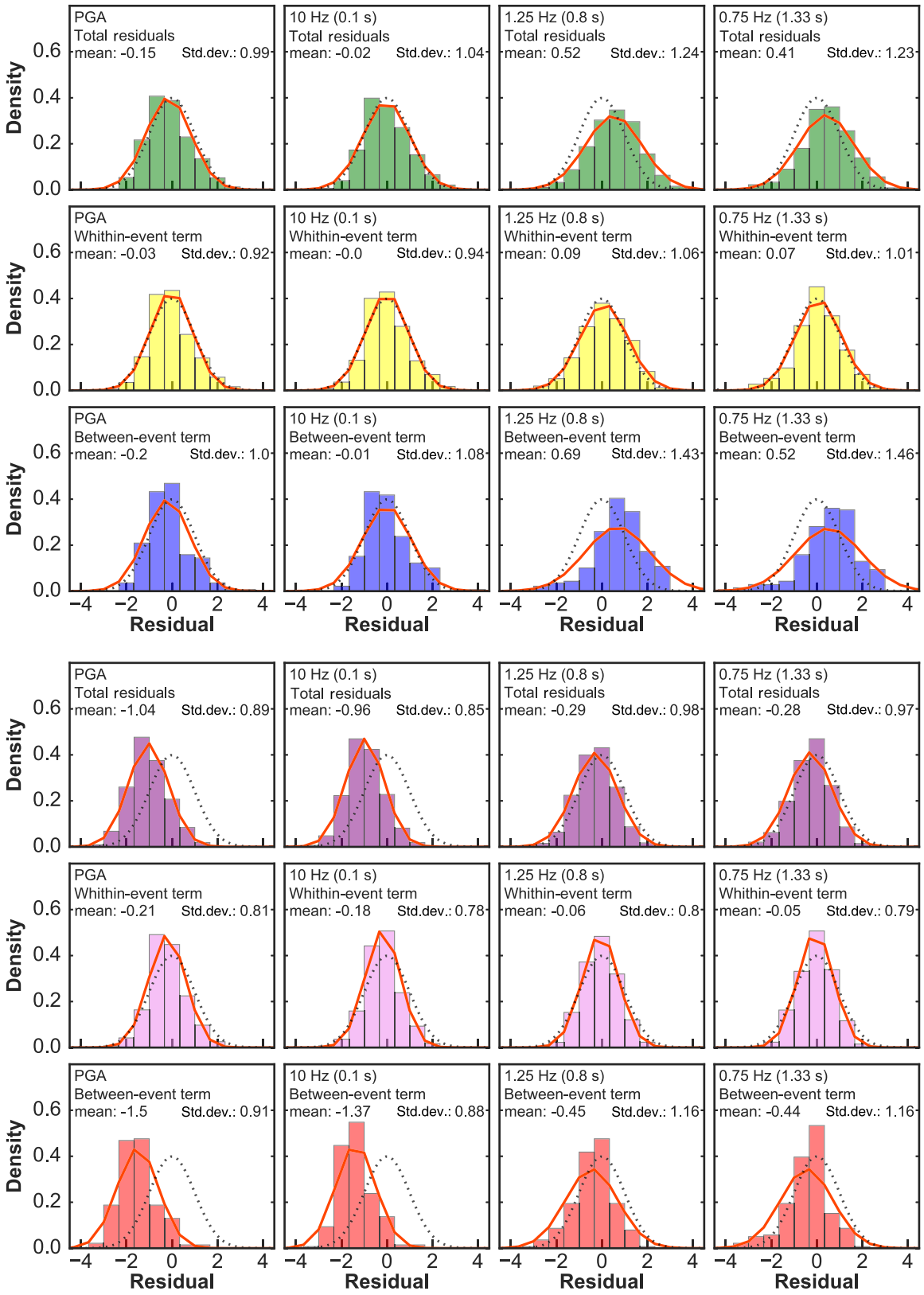

Figure 3. Residual histograms with respect to (top) Abrahamson *et al.* (2016) and (bottom) Montalva *et al.* (2017) ground-motion prediction equations (GMPEs). The dotted line represents the normal density function of the model and the solid line represents the normal density function of the dataset. Columns correspond to the residual distributions for different oscillator periods (peak ground acceleration [PGA], 10, 1.25, and 0.75 Hz), and rows to the total, within-event and between-event residuals. The color version of this figure is available only in the electronic edition.

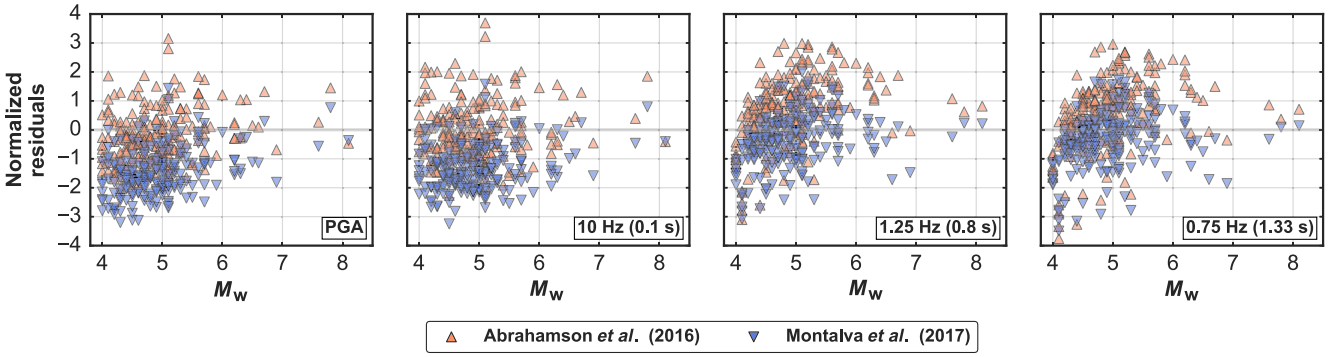

Figure 4. Distribution of computed between-event residuals at different frequencies (PGA, 10, 1.25, and 0.75 Hz) with respect to Montalva *et al.* (2017) (triangles) and Abrahamson *et al.* (2016) (inverted triangles) GMPEs. The residuals do not show any dependency with M_w. The color version of this figure is available only in the electronic edition.

with a rupture plane distance lower than 300 km, to stay in the distance validity range of the GMPEs. Additionally, to avoid bias, the records of the PB11 and PB15 stations have been removed, where possible site effects have been reported (D. Bindi, personal comm., 2015; F. Leyton, personal comm., 2016).

The total residual described above can be separated into between-event and within-event residuals. The first term represents the random effects between events that are not covered by the predictive model and reflects the variation of source factors such as the stress drop or the slip variability in space and time, that cannot be captured by the magnitude and the depth of the source. The within-event residual represents the variation of ground motion at a given distance to the source that comes from the azimuthal variation in the source, the path, and site effects derived from the complexity of the crustal structure, that are not captured by the distance to the source or the site classification (Abrahamson and Youngs, 1992; Strasser *et al.*, 2009, 2010; Al Atik *et al.*, 2010).

The normalized between-event residual of an earthquake i, is given by

$$Z_B^i(T) = \frac{\tau(T) \times \sum_{j=1}^{n} [\log[\mathrm{SA}_{\mathrm{obs}}^{ij}(T)] - \log[\mathrm{SA}_{\mathrm{pred}}^{ij}(T)]]}{n \times \tau(T)^2 + \phi(T)^2}, \tag{3}$$

in which n is the number of records of the event i, $\tau(T)$ and $\phi(T)$ are the standard deviations of the between-event and the within-event residuals of the model for oscillator period T. To reduce the bias, we consider only those between-event residuals of the events that have more than four records with distances to the rupture lower than 300 km.

Consequently, the normalized within-event residuals, for the record j of earthquake i, are defined as

$$Z_W^{ij}(T) = \frac{\log[\mathrm{SA}_{\mathrm{obs}}^{ij}(T)] - \log[\mathrm{SA}_{\mathrm{pred}}^{ij}(T)] - Z_B^i(T) \times \tau(T)}{\phi(T)}. \tag{4}$$

To evaluate the fit of the models to the database, we have first plotted histograms of the distribution of the total, between-event, and within-event residuals with respect to the model's median for the PGA and the three oscillator periods considered (0.1, 0.8, and 1.33 s; Fig. 3). The difference between the standard deviation of the Abrahamson *et al.* (2016) GMPE model and the standard deviation of the residual database, as well as the difference between the median of the model and the median of the residual suggest that the model does not capture the whole variation of strong motions and underestimates their values for medium (0.8 s) and large (1.33 s) oscillator periods. On the other hand, the similar values between standard deviation in the Montalva *et al.* (2017) GMPE model and the standard deviation of the residual database show that this model describes well the variation for the all oscillator periods tested. However, the difference between the median of the model and the median of the residual indicates that the model overestimates the ground motion for low oscillator periods (PGA and 0.1 s).

The fit of the within-event residuals suggests that both models reasonably describe the variability of path and site effects.

The distribution of the between-event residuals suggests that the GMPE of Montalva *et al.* (2017) describes better the variation of source effects for PGA and the three tested oscillator periods. At periods of 0.8 and 1.33 s, the between-event residuals of the Abrahamson *et al.* (2016) model are more scattered than expected from the model.

The between-event residuals distribution does not indicate any magnitude dependency (Fig. 4). Therefore, these two GMPEs can be used as backbone models for the entire magnitude range from $M_w > 4$.

To evaluate the impact of the assumption of a unique value of V_{S30} for the whole network, the site terms (δ_{S2S}) have been computed at each station j for oscillator period T as the mean of the n within-event residuals recorded by the station:

$$\delta_{S2S}^j(T) = \frac{\sum_{i=1}^{n} [Z_W^{ij}(T)]}{n}. \tag{5}$$

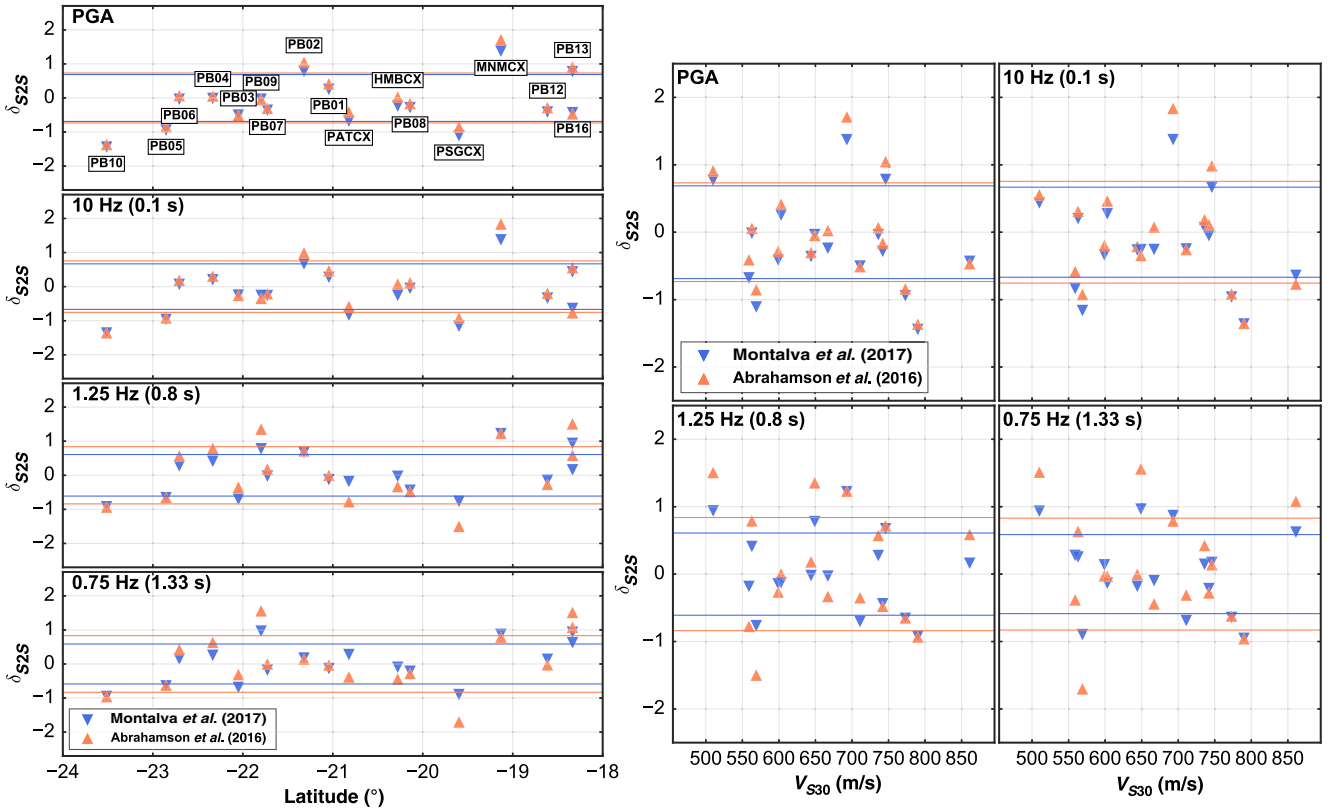

Figure 5. (Left) Stations site terms (δ_{S2S}) at different frequencies according to the Montalva *et al.* (2017) (inverted triangles) and Abrahamson *et al.* (2016) (triangles) GMPEs with respect to the latitude. (Right) Stations site terms (δ_{S2S}) with respect to the V_{S30} obtained by Bastías and Montalva (2016). The horizontal lines represent one standard deviation. No dependency is observed. The color version of this figure is available only in the electronic edition.

The resulting site terms have been compared with inferred V_{S30} values given by Bastías and Montalva (2016). This comparison shows two interesting results: (1) site amplification at IPOC stations do not depend on the latitude (Fig. 5, left), and (2) the correlation between inferred V_{S30} and computed site terms is rather poor (Fig. 5, right). This lack of correlation is consistent with several studies (Chiou and Youngs, 2008; Derras *et al.*, 2016), which have shown that GMPEs using inferred V_{S30} values show large within-event variabilities. These results give further encouragement to promote V_{S30} measurements of IPOC accelerometric stations and also indicate that the north–south variations of between-event residuals are not explained by a systematic regional variation of IPOC site conditions.

As a conclusion, the distribution of residuals suggests that the Montalva *et al.* (2017) model is the best suited for northern Chile and that it can therefore be used as a backbone model to study the spatiotemporal variations of ground motions in this area.

Depth and Regional Dependency of Ground Motions

The evolution of the between-event residual with respect to the depth shows a consistent and significant increase with depth of earthquake radiations at high frequency. This is clearly visible for both regional clusters at low oscillator periods (PGA and 0.1 s), whereas no tendency is observable at medium (0.8 s) or high (1.33 s) oscillator periods (Fig. 6). The distribution of between-event residuals along latitude and depth (Fig. 6, bottom row) shows that for PGA and an oscillator period of 0.1 s, the between-event residuals are clearly differentiated at 40 km depth, where the residual dispersion decreases dramatically and concentrates on higher values. The figure also shows a regional dependency for the medium and high oscillator periods with a lower residual variability and slightly higher residuals values in the northern cluster for earthquakes shallower than 30 km.

To validate the depth dependency of the observed ground motions through between-event residual term distributions, the frequency content of earthquakes have been compared using a Fourier spectral ratio method. This approach has been used recently to compare the frequency content of two subduction earthquakes located at different depths (Lay *et al.*, 2012). Following a similar methodology, we computed the spectral ratios between pairs of earthquakes, using the horizontal Fourier spectra of the acceleration records of the stations that recorded both events.

To apply the method, we used the processed horizontal waveforms to get the Fourier spectra. The Konno and Ohmachi (1998) smoothing function has been applied over each

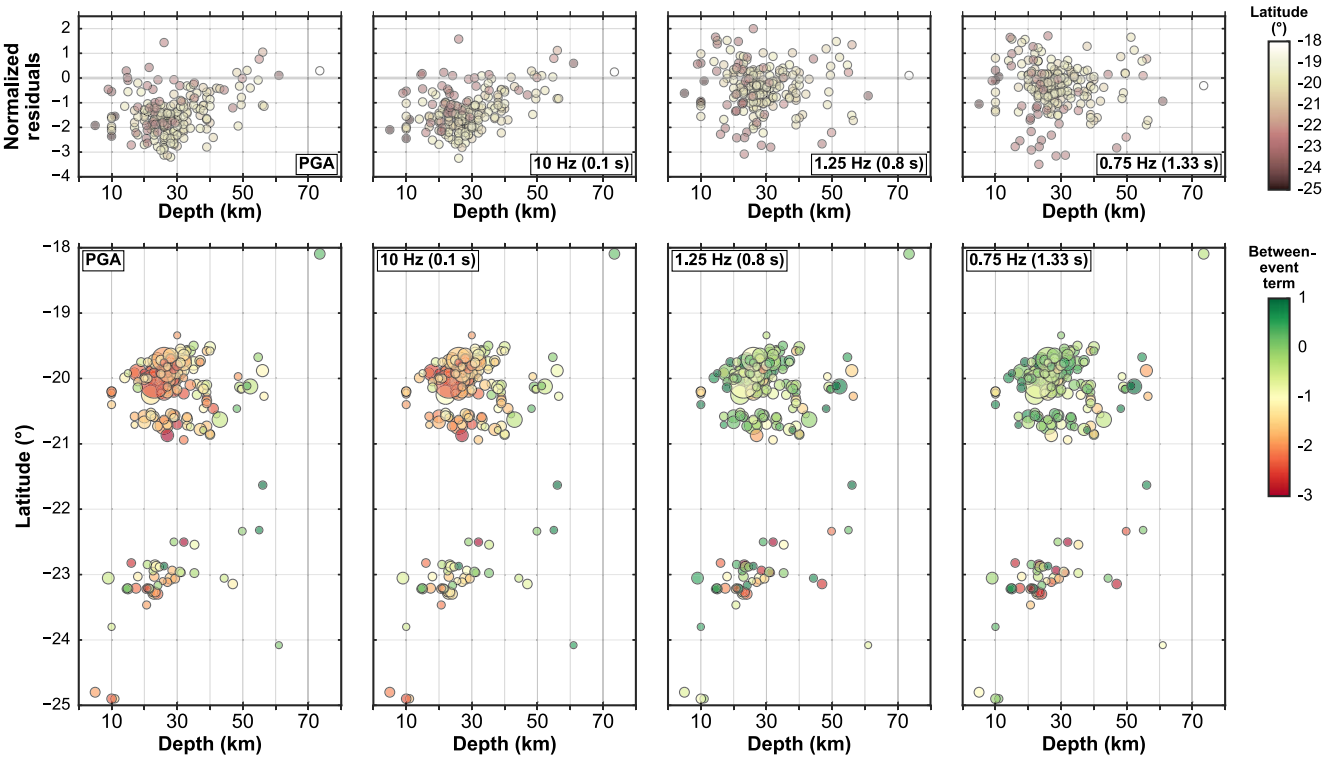

Figure 6. (Top row) Between-event residuals at different oscillator frequencies (PGA, 10, 1.25, and 0.75 Hz) with respect to the Montalva *et al.* (2017) GMPE as a function of the epicentral depth; the fill shows the latitude. An increase of between-event residuals with depth is observable for the PGA and low oscillator periods (0.1 s). (Bottom row) Between-event residuals as a function epicenters latitude and depths. The color version of this figure is available only in the electronic edition.

Fourier spectra and for each station record, both horizontal smoothed Fourier Spectra were then averaged to obtain the horizontal Fourier spectra at each station defined for each frequency f as

$$F_{\mathrm{hor}}(f) = \sqrt{F_{\mathrm{NS}}(f)^2 + F_{\mathrm{EW}}(f)^2}, \tag{6}$$

in which F_{NS} and F_{EW} correspond to the smoothed Fourier spectra of the north–south and east–west acceleration components, respectively, and F_{hor} to the horizontal Fourier spectra.

Then, all spectral ratios obtained at each station for a single pair of earthquakes were averaged with the geometric mean for each frequency; thus, the spectral ratio for each frequency f is defined as

$$\mathrm{SR}_{\mathrm{AB}}(f) = \sqrt[n]{\prod_{j=1}^{n} \frac{F_B^j(f)}{F_A^j(f)}}, \tag{7}$$

in which F_A^j and F_B^j are the horizontal Fourier spectra of events A and B, at the station j, and n is the number of stations that recorded both events.

Pairs of shallow and deep earthquakes with similar magnitudes ($\Delta M_{\mathrm{w}} \leq 0.1$) and relative distance less than 100 km have been selected to compare their frequency contents. The selected pairs of earthquakes consist of one earthquake shallower than 25 km and one earthquake deeper than 40 km. We limited our analysis to earthquakes for which the theoretical hypocenter is located within a distance of 15 km from the subduction interface, as defined by Tassara and Echaurren (2012). We found four earthquakes pairs that meet these criteria. The spectral ratios were calculated as the division of the spectra of the deeper event divided by the spectra of the shallower event (Fig. 7). For all pairs, the spectra amplitude of the deep events is larger than the shallower event for frequencies larger than 1 Hz. This result is in agreement with the depth dependency observed in the GMPE residuals.

The results of both methods presented here are consistent with each other and suggest that interface events below 40 km depth release more energy at high frequencies than shallow interface events for the whole region. In addition, shallow seismicity in the northern part of the seismic gap releases more energy at low frequencies than the seismicity in the southern part of the gap.

Time Dependency of Ground Motions

To evaluate the time variability of the between-event residuals, we focused our analysis on the northern seismicity cluster that is associated with the seismicity of the 2014 M_{w} 8.1 Iquique earthquake (Ruiz *et al.*, 2014; Schurr *et al.*, 2014; Cesca *et al.*, 2016; Kato *et al.*, 2016). We grouped the seismicity into three periods of the seismic cycle bracketing

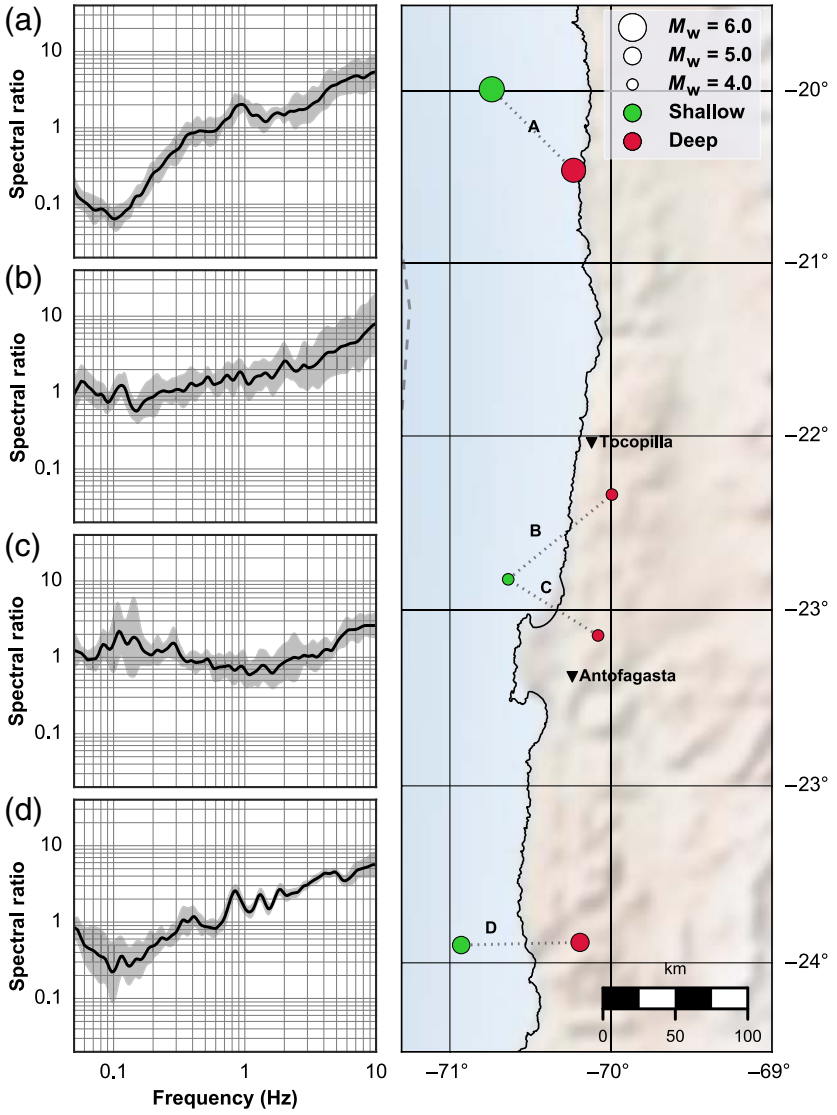

Figure 7. (Left) Spectral ratios computed for pairs of shallow and deep earthquakes. The gray bands show the standard deviation with respect to the geometric mean in the whole frequency band. (Right) Localization of shallow–deep couples. Deep earthquakes generate higher ground-motion amplitudes at frequencies larger than 1 Hz. The color version of this figure is available only in the electronic edition.

the Iquique earthquake (Schurr *et al.*, 2014; Socquet *et al.*, 2017):

1. interseismic: before August 2013
2. preseismic: August 2013–31 March 2014
3. postseismic: after 31 March 2014.

Between-event residual terms are compared in Figure 8 for the three time-period windows at PGA and the three oscillator frequencies selected (10, 1.25, and 0.75 Hz). For PGA and 10 Hz, the between-event residual term decreases from the interseismic to the postseimic period. At frequencies of 1.25 and 0.75 Hz, the between event does not show any important variation from interseismic to preseismic period, and a slight decrease is observed for the postseismic period.

To complement the analysis of the between-event residual variation, the spectral ratio method was again applied (equation 7). Selected pairs of earthquakes of similar magnitude ($\Delta M_w \leq 0.1$), with differences in depths smaller than 20 km and relative distance smaller than 25 km were selected; 425 pairs of earthquakes meet these criteria. The spectral ratios were computed as the division of the most recent event spectrum by the spectrum of the older one. Then, geometrical means of the spectral ratios are divided into three groups:

1. pairs of earthquakes within the interseismic period;
2. pairs of earthquakes belonging to preseismic and interseismic periods; and
3. pairs of earthquakes belonging to postseismic and interseismic periods.

The geometrical means of the spectral ratios over time (Fig. 9) show that at frequencies lower than 1 Hz, the earthquakes of the interseismic period show lower amplitudes than the earthquakes of the preseismic period. Instead, at frequencies higher than 1 Hz, the earthquakes that occur during the intersesimic period show higher amplitudes than the earthquakes that occur during the preseismic period. A similar pattern is also observable when comparing the earthquakes of the interseismic and postseismic periods, although with a lower intensity. The findings are consistent with the variations observed by the GMPEs residual analysis method (Fig. 8).

Discussion

The record of the 2007 Tocopilla and 2014 Iquique seismic sequences by the IPOC network provided a unique dataset in terms quality and quantity (more than 1000 records) to (1) test the performance of the most recent subduction GMPEs and to (2) observe the spatiotemporal variations of the ground motions in a region recognized as a mature seismic gap.

The comparison between the GMPE and the observations suggests that the two tested models are able to describe the ground motion's within-event residuals, which are mainly controlled by site and propagation effects. The main discrepancies between the tested models and the observations are related to the between-event component of the ground-motion variability, which is mainly controlled by source effects.

A possible explanation for this misfit could be due to the limitations of the dataset used to calibrate the ground-motion

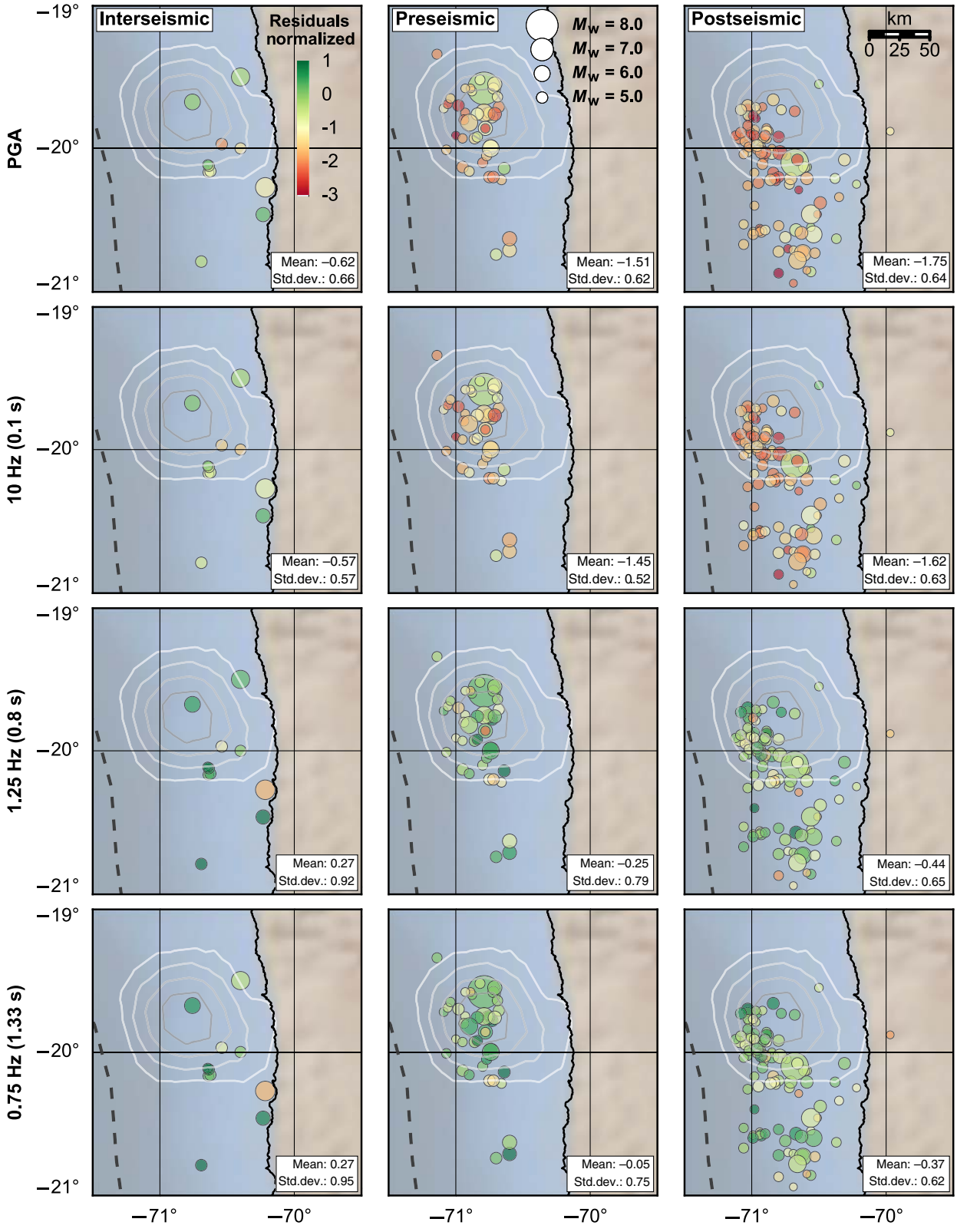

Figure 8. Time and space variability of residuals, at different frequencies (PGA, 10, 1.25, and 0.75 Hz), with respect to the Montalva *et al.* (2017) GMPE for earthquakes between −19° and −21°. Columns correspond to a given period of the seismic cycle period (interseismic before August 2013, preseismic between August 2013 and 31 March 2014, and postseismic after 1 April 2014). The mean and the standard deviation of the between-event residuals showed on each box are indicated in the right bottom corner. Contours lines correspond to the slip distribution of the 1 April 2014 M_w 8.1 Iquique earthquake. PGA and low oscillator period (high frequency, 10 Hz) residuals decrease from interseismic to preseismic time windows. The color version of this figure is available only in the electronic edition.

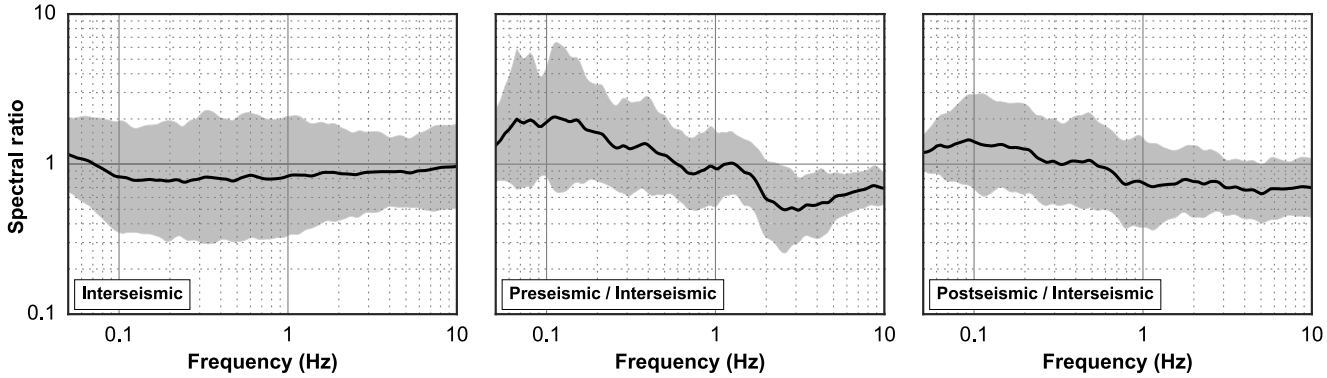

Figure 9. Spectral ratios of similar events ($\Delta M_w \leq 0.1$, interdistance ≤ 25 km), between $-19°$ and $-21°$ of latitude, for the interseismic, preseismic, and postseismic periods associated with the 1 April 2014 Iquique earthquake. The gray bands show the standard deviation (geometric mean) at each frequency.

models. Indeed, the Abrahamson *et al.* (2016) model is based on a global event catalog with a moment magnitude larger than 6, whereas the database used in this study includes earthquakes of smaller magnitude ($4 < M_w < 6$).

The Montalva *et al.* (2017) model has been developed from a seismic catalog with moment magnitudes larger than 5.0 along the entire Chilean trench. This model describes well the ground-motion variability of our dataset. The quality of the fit could then be explained by the inclusion of moderate earthquakes ($5 < M_w < 6$) to calibrate the model.

Our data analysis confirms that the energy radiation pattern of interface earthquakes varies with depth, in agreement with the proposal that the subduction interface is segmented down-dip with different frictional properties characterizing each segment (Lay *et al.*, 2012; Lay, 2015). Such along-dip segmentation is not included so far in the GMPE models. Indeed, engineering ground-motion models predict ground motions for large earthquakes, which break the entire seismogenic zone from small to large (60 km) depths.

Our findings suggest that below 40 km depth, a significant change in the signature of the earthquake spectra exists. This change is coincident with the depth of the contact between the continental Moho and the subduction interface in this area (Patzwahl *et al.*, 1999; Béjar-Pizarro *et al.*, 2010). These two observations are also consistent with the segmentation along depth of the subduction interface and would correspond to the limit between the domains B and C proposed by Lay *et al.* (2012).

The Chilean subduction varies from north to south in terms of mechanical behavior and geometry of the interface (Clift and Vannucchi, 2004; Hoffmann-Rothe *et al.*, 2006; Contreras-Reyes *et al.*, 2010). There is also an influence on the coupling degree that is shown to vary along the trench (Béjar-Pizarro *et al.*, 2010; Métois *et al.*, 2012) and is coherent with the regional segmentation observed for the between-event residuals at medium and long oscillator periods for seismicity shallower than 40 km depth (Fig. 6, bottom row).

Several past crustal earthquakes studies (i.e., Abrahamson *et al.*, 2008) have suggested that aftershocks generate weaker ground motions than the associated mainshock. Our results have shown that the ground motions have started to change several months before the occurrence of 2014 Iquique earthquake, with a progressive decrease of the released energy at high frequencies. This observation may indicate a change on the subduction interface that may be related to a long-term nucleation process of the megathrust earthquake (Socquet *et al.*, 2017). The ground-motion temporal variation is consistent in time with aseismic slip around the rupture area of the 2014 Iquique earthquake and a slow migration of the foreshock activity (Kato and Nakagawa, 2014; Schurr *et al.*, 2014; Kato *et al.*, 2016; Socquet *et al.*, 2017), similarly to what has been observed before the 2011 M_w 9.1 Tohoku-Oki earthquake (Mavrommatis *et al.*, 2015; Yokota and Koketsu, 2015). This observation sheds light on the potential processes that occur on the subduction interface through the seismic cycle.

Stress-drop inversions have been used for years by the seismological community to analyze the physics of earthquakes. The stress drop, being proportional to the cube of the corner frequency, is sensitive to the uncertainty in the corner frequency (e.g., Cotton *et al.*, 2013). Our study suggests that the analysis of GMPE between-event residuals could also be used not only for engineering purposes but also to analyze the source characteristics of earthquakes. Indeed, these residuals take into account both the magnitude effect and the propagation effect (through the functional form of the GMPE), and it has been shown that response between-event residuals are highly correlated with classical Fourier spectrum based stress drop (e.g., Bindi *et al.*, 2007). Between-event residuals analysis may therefore constitute a new possibility to compare source effects of earthquakes with various magnitude and locations.

Finally, the consistency of the results with other studies opens the possibility to use parameters such as the between-event residuals, stress drop, earthquake spectra, and strong motion, as a proxy for the variability of the frictional properties of the subduction interface.

Conclusion

Testing the GMPEs models is a necessary contribution to seismic hazard assessment in areas that have been recently instrumented. For the specific case of northern Chile, the results presented in this study have shown that the combination of the Abrahamson *et al.* (2016) and Montalva *et al.* (2017) models show different strengths and weaknesses. These two models successfully predict the median values and capture the variability of the ground motions generated by the interface seismicity in different frequency bands, even for a dataset extended out of the validity range of M_w in both models. The results have shown that for a dataset including earthquakes of M_w as low as 4.0, the Abrahamson *et al.* (2016) model fits observations better for low oscillator periods (0.8 and 1.33 s), whereas the Montalva *et al.* (2017) model is more suitable for medium and high oscillator periods (PGA and 0.1 s). Considering all frequencies and the magnitude range, which is important from a seismic hazard point of view ($M_w > 5$), the Montalva *et al.* (2017) model is the best suited for northern Chile.

The southern part of the north Chile seismic gap shows weaker ground motions at low frequencies than the northern part of the gap. This suggests a lateral segmentation of the subduction interface such an along-strike segmentation has also been shown by studies of interseismic coupling (Béjar-Pizarro *et al.*, 2013; Métois *et al.*, 2013; Li *et al.*, 2015). This suggests a potential link between the state of coupling during the interseismic phase, the energy radiation characteristics of interface earthquakes, and the friction on the subduction interface that requires further investigations. In addition, using two different methods (GMPE residuals and the spectral ratios), we showed that the observed ground motions increase with hypocentral depth for interface subduction earthquakes. This suggests that the event depth must be considered in the development of future GMPE to include in the models interface subduction earthquakes of moderate magnitudes, which are not rupturing the entire seismogenic interface. This could extend the use of the GMPE as backbone ground motion to study the properties of the subduction interface. Also, this depth dependency confirms previous observations of along-dip segmentation of the subduction megathrust seen in the values of interseismic coupling (Béjar-Pizarro *et al.*, 2010; Lay *et al.*, 2012) and in the geometry because an abrupt change in the subduction angle has been documented in the area (Contreras-Reyes *et al.*, 2012).

Ground motions have also been shown to vary through time by both methods presented in this work (GMPEs and spectral ratios). The time dependency can be related to the earthquake cycle and has been observed by studying in great details the seismic events associated with the 2014 Iquique megathrust earthquake. Although a significant change in the earthquake frequency content before and after the mainshock can be expected, this is not what we observe. Instead, the data show that the change occurs several months before the mainshock and is characterized by a progressive decrease of interface earthquake energy release at high frequencies. This change has been shown to concur with an eight-month slow-slip event on the subduction interface, and has been interpreted as the long-term nucleation process of the 2014 megathrust earthquake (Socquet *et al.*, 2017).

Finally, the dependencies detected on the between-event term open the possibility to incorporate new factors to improve ground-motion models in the future. An important factor to improve the predictability of the GMPE models is to better take into account depth and regional variations.

Data and Resources

All strong-motion data used in this work have been recorded by the CX-network of the Integrated Plate boundary Observatory Chile (http://www.ipoc-network.org). These data are available to registered users at the GEOFON repository (http://geofon.gfz-potsdam.de/waveform/archive/network.php?ncode=CX). The Global Centroid Moment Tensor (CMT) and the moment tensor solutions are freely available (http://www.globalcmt.org/CMTsearch.html) as well the GEOFON bulletin information (http://geofon.gfz-potsdam.de/eqinfo/eqinfo.php). All of the above websites were last accessed on June 2016.

Acknowledgments

This work has been possible thanks to the contribution of the Integrated Plate boundary Observatory Chile (IPOC) consortium that has facilitated the access to the CX-network ground-motion data, of Bernd Schurr that has facilitated the focal mechanism catalog of GEOFON data center, of Dino Bindi and the two anonymous reviewers that contributed with their helpful comments on the article, and to the BecasChile scholarship program by the Chilean National Commission of Science and Technology (CONICYT).

References

Abrahamson, N., G. Atkinson, D. Boore, Y. Bozorgnia, K. Campbell, B. Chiou, I. Idriss, W. Silva, and R. Youngs (2008). Comparisons of the NGA ground-motion relations, *Earthq. Spectra* **24,** 45–66.

Abrahamson, N., N. Gregor, and K. Addo (2016). BC Hydro ground motion prediction equations for subduction earthquakes, *Earthq. Spectra* **32,** 23–44, doi: 10.1193/051712EQS188MR.

Abrahamson, N. A., and R. R. Youngs (1992). A stable algorithm for regression analyses using the random effects model, *Bull. Seismol. Soc. Am.* **82,** 505–510.

Akkar, S., M. A. Sandıkkaya, M. Şenyurt, A. Azari Sisi, B. Ö. Ay, P. Traversa, J. Douglas, F. Cotton, L. Luzi, B. Hernandez, *et al.* (2014). Reference database for seismic ground-motion in Europe (RESORCE), *Bull. Earthq. Eng.* **12,** 311–339, doi: 10.1007/s10518-013-9506-8.

Al Atik, L., N. Abrahamson, J. J. Bommer, F. Scherbaum, F. Cotton, and N. Kuehn (2010). The variability of ground-motion prediction models and its components, *Seismol. Res. Lett.* **81,** 794–801, doi: 10.1785/gssrl.81.5.794.

Arango, M. C., F. O. Strasser, J. J. Bommer, R. Boroschek, D. Comte, and H. Tavera (2011). A strong-motion database from the Peru–Chile subduction zone, *J. Seismol.* **15,** 19–41, doi: 10.1007/s10950-010-9203-x.

Argus, D. F., R. G. Gordon, and C. DeMets (2011). Geologically current motion of 56 plates relative to the no-net-rotation reference frame, *Geochem. Geophys. Geosys.* **12,** no. 11, doi: 10.1029/2011GC003751.

Astiz, L., T. Lay, and H. Kanamori (1988). Large intermediate-depth earthquakes and the subduction process, *Phys. Earth Planet. In.* **53,** 80–166.

Bastías, N., and G. A. Montalva (2016). Chile strong ground motion flatfile, *Earthq. Spectra* **32,** 2549–2566, doi: 10.1193/102715eqs158dp.

Béjar-Pizarro, M., D. Carrizo, A. Socquet, R. Armijo, S. Barrientos, F. Bondoux, S. Bonvalot, J. Campos, D. Comte, J. B. de Chabalier, *et al.* (2010). Asperities and barriers on the seismogenic zone in north Chile: State-of-the-art after the 2007 M_w 7.7 Tocopilla earthquake inferred by GPS and InSAR data, *Geophys. J. Int.* **183,** 390–406, doi: 10.1111/j.1365-246X.2010.04748.x.

Béjar-Pizarro, M., A. Socquet, R. Armijo, D. Carrizo, J. Genrich, and M. Simons (2013). Andean structural control on interseismic coupling in the north Chile subduction zone, *Nature Geosci.* **6,** 462–467.

Bindi, D., S. Parolai, H. Grosser, C. Milkereit, and E. Durukal (2007). Empirical ground-motion prediction equations for northwestern Turkey using the aftershocks of the 1999 Kocaeli earthquake, *Geophys. Res. Lett.* **34,** no. 8, doi: 10.1029/2007GL029222.

Boore, D. M., and J. J. Bommer (2005). Processing of strong-motion accelerograms: Needs, options and consequences, *Soil Dynam. Earthq. Eng.* **25,** 93–115, doi: 10.1016/j.soildyn.2004.10.007.

Bouchon, M., V. Durand, D. Marsan, H. Karabulut, and J. Schmittbuhl (2013). The long precursory phase of most large interplate earthquakes, *Nature Geosci.* **6,** 299–302.

Cesca, S., F. Grigoli, S. Heimann, T. Dahm, M. Kriegerowski, M. Sobiesiak, C. Tassara, and M. Olcay (2016). The M_w 8.1 2014 Iquique, Chile, seismic sequence: A tale of foreshocks and aftershocks, *Geophys. J. Int.* **204,** 1766–1780, doi: 10.1093/gji/ggv544.

Chiou, B.-J., and R. R. Youngs (2008). An NGA model for the average horizontal component of peak ground motion and response spectra, *Earthq. Spectra* **24,** 173–215, doi: 10.1193/1.2894832.

Clift, P., and P. Vannucchi (2004). Controls on tectonic accretion versus erosion in subduction zones: Implications for the origin and recycling of the continental crust, *Rev. Geophys.* **42,** no. 2, doi: 10.1029/2003RG000127.

Contreras-Reyes, E., E. R. Flueh, and I. Grevemeyer (2010). Tectonic control on sediment accretion and subduction off south central Chile: Implications for coseismic rupture processes of the 1960 and 2010 megathrust earthquakes, *Tectonics* **29,** no. TC6018, doi: 10.1029/2010TC002734.

Contreras-Reyes, E., J. Jara, I. Grevemeyer, S. Ruiz, and D. Carrizo (2012). Abrupt change in the dip of the subducting plate beneath north Chile, *Nature Geosci.* **5,** 342–345.

Cotton, F., R. Archuleta, and M. Causse (2013). What is sigma of the stress drop? *Seismol. Res. Lett.* **84,** 42–48, doi: 10.1785/0220120087.

Delouis, B., M. Pardo, D. Legrand, and T. Monfret (2009). The M_w 7.7 Tocopilla earthquake of 14 November 2007 at the southern edge of the northern Chile seismic gap: Rupture in the deep part of the coupled plate interface, *Bull. Seismol. Soc. Am.* **99,** 87–94, doi: 10.1785/0120080192.

Derras, B., P.-Y. Bard, and F. Cotton (2016). Site-condition proxies, ground motion variability, and data-driven GMPEs: Insights from the NGA-West2 and RESORCE data sets, *Earthq. Spectra* **32,** 2027–2056.

Fuenzalida, A., B. Schurr, M. Lancieri, M. Sobiesiak, and R. Madariaga (2013). High-resolution relocation and mechanism of aftershocks of the 2007 Tocopilla (Chile) earthquake, *Geophys. J. Int.* **194,** 1216–1228, doi: 10.1093/gji/ggt163.

Gusman, A. R., S. Murotani, K. Satake, M. Heidarzadeh, E. Gunawan, S. Watada, and B. Schurr (2015). Fault slip distribution of the 2014 Iquique, Chile, earthquake estimated from ocean-wide tsunami waveforms and GPS data, *Geophys. Res. Lett.* **42,** 1053–1060.

Haendel, A., S. Specht, N. M. Kuehn, and F. Scherbaum (2014). Mixtures of ground-motion prediction equations as backbone models for a logic tree: An application to the subduction zone in northern Chile, *Bull. Earthq. Eng.* **13,** 483–501, doi: 10.1007/s10518-014-9636-7.

Hayes, G. P., M. W. Herman, W. D. Barnhart, K. P. Furlong, S. Riquelme, H. M. Benz, E. Bergman, S. Barrientos, P. S. Earle, and S. Samsonov (2014). Continuing megathrust earthquake potential in Chile after the 2014 Iquique earthquake, *Nature* **512,** 295–298.

Heuret, A., S. Lallemand, F. Funiciello, C. Piromallo, and C. Faccenna (2011). Physical characteristics of subduction interface type seismogenic zones revisited, *Geochem. Geophys. Geosys.* **12,** no. 1, doi: 10.1029/2010GC003230.

Hoffmann-Rothe, A., N. Kukowski, G. Dresen, H. Echtler, O. Oncken, J. Klotz, E. Scheuber, and A. Kellner (2006). Oblique convergence along the Chilean margin: Partitioning, margin-parallel faulting and force interaction at the plate interface, in *The Andes: Active Subduction Orogeny*, O. Oncken, G. Chong, G. Franz, P. Giese, H.-J. Götze, V. A. Ramos, M. R. Strecker, and P. Wigger (Editors), Springer-Verlag, Berlin/Heidelberg, Germany, 125–146.

Kanamori, H. (1986). Rupture process of subduction-zone earthquakes, *Annu. Rev. Earth Planet. Sci.* **14,** 293.

Kato, A., and S. Nakagawa (2014). Multiple slow-slip events during a foreshock sequence of the 2014 Iquique, Chile M_w 8.1 earthquake, *Geophys. Res. Lett.* **41,** 5420–5427.

Kato, A., J. i. Fukuda, T. Kumazawa, and S. Nakagawa (2016). Accelerated nucleation of the 2014 Iquique, Chile M_w 8.2 earthquake, *Sci. Rept.* **6,** Article Number 24792, doi: 10.1038/srep24792.

Konno, K., and T. Ohmachi (1998). Ground-motion characteristics estimated from spectral ratio between horizontal and vertical components of microtremor, *Bull. Seismol. Soc. Am.* **88,** 228–241.

Lay, T. (2015). The surge of great earthquakes from 2004 to 2014, *Earth Planet. Sci. Lett.* **409,** 133–146.

Lay, T., H. Kanamori, C. J. Ammon, K. D. Koper, A. R. Hutko, L. Ye, H. Yue, and T. M. Rushing (2012). Depth-varying rupture properties of subduction zone megathrust faults, *J. Geophys. Res.* **117,** no. B4, doi: 10.1029/2011JB009133.

Leyton, F., C. Pastén, G. Montalva, G. Hurtado, A. Leopold, S. Ruiz, and E. Saéz (2017). Towards a geophysical characterization of the Chilean seismological stations, *16th World Conf. on Earthquake Engineering*, Santiago, Chile, 9–13 January 2017.

Li, S., M. Moreno, J. Bedford, M. Rosenau, and O. Oncken (2015). Revisiting viscoelastic effects on interseismic deformation and locking degree: A case study of the Peru–North Chile subduction zone, *J. Geophys. Res.* **120,** 4522–4538.

Lomnitz, C. (2004). Major earthquakes of Chile: A historical survey, 1535–1960, *Seismol. Res. Lett.* **75,** 368–378.

Mavrommatis, A. P., P. Segall, N. Uchida, and K. M. Johnson (2015). Long-term acceleration of aseismic slip preceding the M_w 9 Tohoku-oki earthquake: Constraints from repeating earthquakes, *Geophys. Res. Lett.* **42,** 9717–9725.

Métois, M., A. Socquet, and C. Vigny (2012). Interseismic coupling, segmentation and mechanical behavior of the central Chile subduction zone, *J. Geophys. Res.* **117,** no. B3, doi: 10.1029/2011JB008736.

Métois, M., A. Socquet, C. Vigny, D. Carrizo, S. Peyrat, A. Delorme, E. Maureira, M.-C. Valderas-Bermejo, and I. Ortega (2013). Revisiting the north Chile seismic gap segmentation using GPS-derived interseismic coupling, *Geophys. J. Int.* **194,** 1283–1294.

Métois, M., C. Vigny, and A. Socquet (2016). Interseismic coupling, megathrust earthquakes and seismic swarms along the Chilean subduction zone (38°–18°S), *Pure Appl. Geophys.* **173,** 1431–1449, doi: 10.1007/s00024-016-1280-5.

Montalva, G. A., N. Bastías, and A. Rodriguez-Marek (2017). Ground-motion prediction equation for the Chilean subduction zone, *Bull. Seismol. Soc. Am.* **107,** no. 2, doi: 10.1785/0120160221.

Motagh, M., B. Schurr, J. Anderssohn, B. Cailleau, T. R. Walter, R. Wang, and J.-P. Villotte (2010). Subduction earthquake deformation associated with 14 November 2007, M_w 7.8 Tocopilla earthquake in Chile: Results from InSAR and aftershocks, *Tectonophysics* **490,** 60–68.

Nigam, N. C., and P. C. Jennings (1969). Calculation of response spectra from strong-motion earthquake records, *Bull. Seismol. Soc. Am.* **59,** 909–922.

Ozawa, S., T. Nishimura, H. Munekane, H. Suito, T. Kobayashi, M. Tobita, and T. Imakiire (2012). Preceding, coseismic, and postseismic slips of

the 2011 Tohoku earthquake, Japan, *J. Geophys. Res.* **117,** no. B7, doi: 10.1029/2011JB009120.

Patzwahl, R., J. Mechie, A. Schulze, and P. Giese (1999). Two-dimensional velocity models of the Nazca plate subduction zone between 19.5°S and 25°S from wide-angle seismic measurements during the CINCA95 project, *J. Geophys. Res.* **104,** 7293–7317.

Peyrat, S., R. Madariaga, E. Buforn, J. Campos, G. Asch, and J. Vilotte (2010). Kinematic rupture process of the 2007 Tocopilla earthquake and its main aftershocks from teleseismic and strong-motion data, *Geophys. J. Int.* **182,** 1411–1430.

Ruiz, S., M. Metois, A. Fuenzalida, J. Ruiz, F. Leyton, R. Grandin, C. Vigny, R. Madariaga, and J. Campos (2014). Intense foreshocks and a slow slip event preceded the 2014 Iquique M_w 8.1 earthquake, *Science* **345,** 1165–1169, doi: 10.1126/science.1256074.

Schurr, B., G. Asch, S. Hainzl, J. Bedford, A. Hoechner, M. Palo, R. Wang, M. Moreno, M. Bartsch, Y. Zhang, *et al.* (2014). Gradual unlocking of plate boundary controlled initiation of the 2014 Iquique earthquake, *Nature* **512,** 299–302, doi: 10.1038/nature13681.

Schurr, B., G. Asch, M. Rosenau, R. Wang, O. Oncken, S. Barrientos, P. Salazar, and J. P. Vilotte (2012). The 2007 M 7. 7 Tocopilla northern Chile earthquake sequence: Implications for along-strike and downdip rupture segmentation and megathrust frictional behavior, *J. Geophys. Res.* **117,** no. B5, doi: 10.1029/2011JB009030.

Socquet, A., J. Piña-Valdes, J. Jara, F. Cotton, A. Walpersdorf, N. Cotte, S. Specht, F. Ortega-Culaciati, D. Carrizo, and E. Norabuena (2017). An 8 month slow slip event triggers progressive nucleation of the 2014 Chile megathrust, *Geophys. Res. Lett.* **44,** no. 9, 4046–4053.

Specht, S., O. Heidbach, F. Cotton, and A. Zang (2017). Data-driven earthquake focal mechanism cluster analysis, *Scientific Technical Report STR, 17/01*, GFZ German Research Centre for Geosciences, Potsdam, Germany.

Strasser, F. O., N. A. Abrahamson, and J. J. Bommer (2009). Sigma: Issues, insights, and challenges, *Seismol. Res. Lett.* **80,** 40–56, doi: 10.1785/gssrl.80.1.40.

Strasser, F. O., M. C. Arango, and J. J. Bommer (2010). Scaling of the source dimensions of interface and intraslab subduction-zone earthquakes with moment magnitude, *Seismol. Res. Lett.* **81,** 941–950, doi: 10.1785/gssrl.81.6.941.

Tassara, A., and A. Echaurren (2012). Anatomy of the Andean subduction zone: Three-dimensional density model upgraded and compared against global-scale models, *Geophys. J. Int.* **189,** 161–168, doi: 10.1111/j.1365-246X.2012.05397.x.

Tichelaar, B. W., and L. J. Ruff (1993). Depth of seismic coupling along subduction zones, *J. Geophys. Res.* **98,** 2017–2037.

Yokota, Y., and K. Koketsu (2015). A very long-term transient event preceding the 2011 Tohoku earthquake, *Nature Comm.* **6,** 5934.

Youngs, R. R., N. Abrahamson, F. I. Makdisi, and K. Sadigh (1995). Magnitude-dependent variance of peak ground acceleration, *Bull. Seismol. Soc. Am.* **85,** 1161–1176.

Youngs, R. R., S.-J. Chiou, W. J. Silva, and J. R. Humphrey (1997). Strong ground motion attenuation relationships for subduction zone earthquakes, *Seismol. Res. Lett.* **68,** 58–73, doi: 10.1785/gssrl.68.1.58.

Zhao, J. X., J. Zhang, A. Asano, Y. Ohno, T. Oouchi, T. Takahashi, H. Ogawa, K. Irikura, H. K. Thio, P. G. Somerville, *et al.* (2006). Attenuation relations of strong ground motion in Japan using site classification based on predominant period, *Bull. Seismol. Soc. Am.* **96,** 898–913, doi: 10.1785/0120050122.

Univ. Grenoble Alpes, Univ. Savoie Mont Blanc
CNRS, IRD, IFSTTAR
ISTerre
38000 Grenoble
France
jesus.pina-valdes@univ-grenoble-alpes.fr
anne.socquet@univ-grenoble-alpes.fr
(J.P.-V., A.S.)

Helmholtz Centre Potsdam
GFZ German Research Institute for Geosciences
Helmholtzstrasse 6
14467 Potsdam
Germany
fcotton@gfz-potsdam.de
(F.C.)

Institute of Earth and Environmental Science
University of Potsdam
Karl-Liebknecht-Straße 24-25
14476 Potsdam-Golm
Germany
sspecht@uni-potsdam.de
(S.S.)

Manuscript received 14 February 2017;
Published Online 27 February 2018